

Externally-resonated linear micro vibromotor for micro assembly

Kazuhiro Saitou^a and Soungjin J. Wou

Department of Mechanical Engineering and Applied Mechanics
University of Michigan, Ann Arbor, MI 48109-2125, USA

ABSTRACT

A new design of a linear micro vibromotor for on-substrate fine positioning of micro-scale components is presented where a micro linear slider is actuated by vibratory impacts exerted by micro cantilever impacters. These micro cantilever impacters are *selectively* resonated by shaking the entire substrate with a piezoelectric vibrator, requiring no need for built-in driving mechanisms such as electrostatic comb actuators as reported previously.^{1,2} This selective resonance of the micro cantilever impacters via an external vibration energy field³ provides with a very simple means of controlling forward and backward motion of the micro linear slider, facilitating *assembly and disassembly* of a micro component on a substrate. The double-V beam suspension design⁴ is employed in the micro cantilever impacters for larger displacement in the lateral direction while achieving higher stiffness in the transversal direction. An analytical model of the device is derived in order to obtain, through the Simulated Annealing algorithm, an optimal design which maximizes translation speed of the linear slider at desired external input frequencies. Prototypes of the externally-resonated linear micro vibromotor are fabricated using the three-layer polysilicon surface micro machining process provided by the MCNC MUMPS service.

Keywords: micro assembly, on-substrate fine positioning, micro electro-mechanical systems (MEMS), micro linear vibromotor, micro mechanical resonator.

1. INTRODUCTION

Assembly has not been an issue of research in micro electro mechanical systems (MEMS). This is because one of the largest advantages of surface micro fabrication technologies, which MEMS is based on, is no need for assembly; an entire system (*e.g.*, a chip) with multiple components can be fabricated in processes involving no assembly. As the complexity of the system increases, however, the need for assembly, as well as disassembly, becomes more evident since complex integrated systems often suffer from low reliability due to the lack of modularity among subsystems. This is especially true for MEMS, which often require complex electro mechanical integration and packaging. Despite these demands, no practical assembly/disassembly methods of micro-scale components suitable for automation has been developed so far.

Assembly in MEMS, if needed, is typically done by manual operation of micro probes or micro tweezers (*e.g.*,⁵). Such miniaturization of the conventional pick-and-place robotic assembly, however, experiences extreme difficulty in handling and positioning components with sizes less than a millimeter, due to the surface adhesion forces which cause sticking among components and handling devices.⁶ Figure 1 illustrates pick-and-place assembly of a micro-scale component using a micro gripper. Surface adhesion forces such as electrostatic, van der Waals, and surface tension forces cause the component to stick to the gripper during the approach (Figure 1 (b)) and the release (Figure 1 (d)) phases. Mechanical shock can be applied to the gripper to drop the stuck component (Figure 1 (e)), with the price of inaccurate positioning of the released component (Figure 1 (f)).

One way to overcome this problem is to design a device on the substrate that facilitates component positioning so that gross positioning is done in the conventional pick-and-place fashion*, whereas fine positioning is done by the on-substrate positioning device. This concept is illustrated in Figure 2, where a on-substrate linear actuator pushes a inaccurately positioned micro component (*e.g.*, as a result of the “shock release” shown in Figure 1 (e) and (f)) against a fixture anchored to the substrate (Figure 2 (a)), achieving precise positioning of the component (Figure 2 (b)). The linear actuator also should be able to re-open to release the positioned component to facilitate the potential needs for disassembly (Figure 2 (c)).

^a Corresponding author; Phone: (734) 763-0036, Fax: (734) 647-3170, E-mail: kazu@umich.edu

*or with other processes which are more effective for gross positioning – see Section 5 for an example.

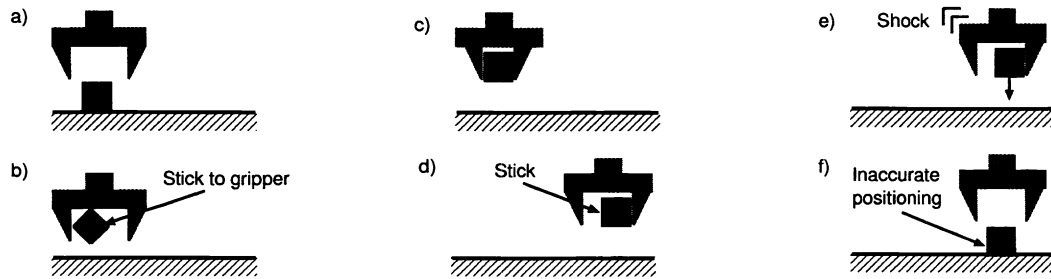


Figure 1. Typical pick-and-place assembly in micro scale (modified from⁶). (a) A gripper approaches to a component; (b) The component sticks to the gripper; (c) the gripper grasps the component; (d) The component is transported to a desired location; (e) The component is released with shock; (f) The component is placed at inaccurate position.

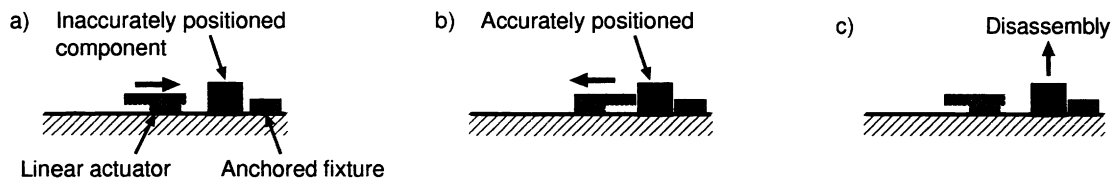


Figure 2. Precise component positioning and release with a on-substrate linear actuator and a fixture. (a) inaccurately positioned component; (b) accurately positioned component; (c) release of the component for disassembly.

This paper describes a design of such a micro linear actuator for fine positioning of a micro- to meso-scale component on a substrate. The design is based on a linear micro vibromotor reported by Daneman *et al.*,¹ where a micro linear slider is actuated by vibratory impacts exerted by micro cantilever impacters. Dissimilar to their design, however, these micro cantilever impacters are *selectively* resonated by shaking the entire substrate with a piezoelectric vibrator, requiring no need for built-in driving mechanisms such as electrostatic comb actuators. This selective resonance of the micro cantilever impacters via an external vibration energy field³ provides with a very simple means of controlling forward and backward motion of the micro linear slider, facilitating *assembly and disassembly* of a micro component on a substrate. The double-V beam suspension design⁴ is employed in the micro cantilever impacters for larger displacement in the lateral direction while achieving higher stiffness in the transversal direction. An analytical model of the device is derived in order to obtain, through the Simulated Annealing algorithm, an optimal design which maximizes translation speed of the linear slider at desired external input frequencies. Prototypes of the externally-resonated linear micro vibromotor are fabricated using the three-layer polysilicon surface micro machining process provided by the MCNC MUMPS service.

2. RELATED WORK

In the efforts of the development of a bulk assembly method for micro- to meso-scale components, several approaches have been proposed to incorporate *self-positioning* to micro assembly. Yeh and Smith⁷ integrated trapezoidal GaAs micro blocks on a Si substrate with trapezoidal holes by dispensing these in a carrier fluid (ethanol) onto the Si substrate. Cohn, Kim and Pisano⁸ experimented with the self-assembly of small hexagonal parts (1 mm in diameter) by placing a quantity of them on a slightly concave diaphragm that was agitated with a loudspeaker. Hosokawa, Shimoyama and Miura⁹ experimented with the self-assembly of micro parts which are brought together on a water surface by surface tension of the water. Böhringer, Goldberg, Cohn, Howe and Pisano¹⁰ proposed a method to position sub-millimeter parts using ultrasonic vibration to eliminate friction and adhesion, and electrostatic forces to position and align parts in parallel. While no external positioning/handling of components is necessary in these

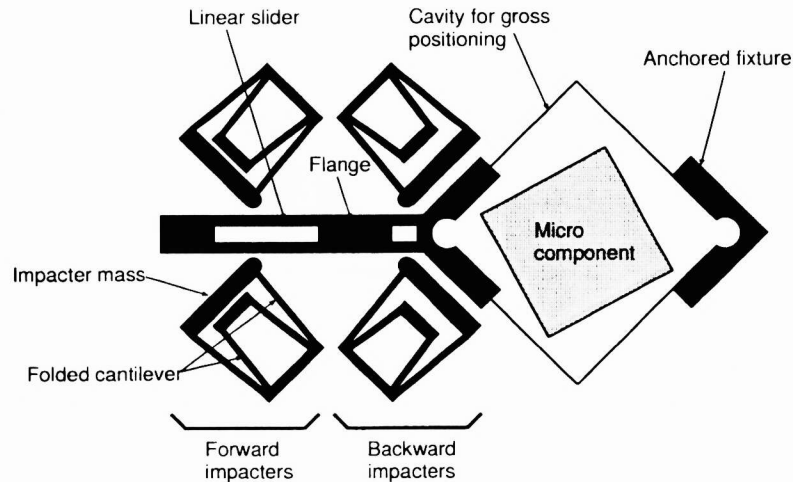


Figure 3. A schematic top view of the externally-resonated linear micro vibromotor for on-substrate precise positioning.

methods, the components are only grossly positioned, requiring auxiliary means to achieve precise positioning needed for practical micro electro mechanical applications.

Other work has been done on the use of mechanical force to both self-position and fasten components so that assembly requires *less* positioning/handling of components. Judy, Cho, Howe and Pisano¹¹ fabricated a laterally-deflecting cantilever on the side wall of a polysilicon mesa which adjusts the position of other structures attaching to the cantilever, and provides the bearing forces between structures. Burgett, Pister and Fearing¹² used spring loaded latches to self-position the plates within micro fabricated hinges. Prasad, Böhringer and MacDonald¹³ fabricated a micro snap fastener with 1–2 μm wide laterally-deflecting chamfered latches. These methods do not consider the potential need for disassembly, hence non-destructive removal of the fastened components is extremely difficult or even impossible.

3. DESIGN

3.1. Operational principle

Our design of the externally-resonated linear micro vibromotor for micro assembly is based on a linear micro vibromotor reported by Daneman *et al.*,¹ where a micro linear slider is actuated by vibratory impacts exerted by micro cantilever impacters. Dissimilar to their design, however, these micro cantilever impacters are selectively resonated by *external* piezoelectric vibration, requiring no need for built-in driving mechanisms such as electrostatic comb actuators.

As illustrates in Figure 3, it consists of a linear slider located between two pairs of folded cantilever impacters anchored on the substrate which can exert forward and backward vibratory impacts to the sides of the slider, depending on which pair of impacters is resonated by external vibration. Figure 4 illustrates the three-step operation of the linear micro vibromotor. First, the substrate is shaken with a piezoelectric vibrator at the frequency f_1 . This external vibration resonates *only* the forward impacters, causing the linear slider to move right (Figure 4 (a)). This motion causes the slider to push a micro component against an anchored fixture, achieving precise positioning (Figure 4 (b)). Next, the substrate is shaken at the frequency f_2 . This external vibration resonates *only* the backward impacters and moves the slider to the left (Figure 4 (c)), releasing the positioned component.

This selective resonance of the micro cantilever impacters via an external vibration energy field³ provides with very simple means of controlling forward and backward motion of the micro linear slider, without explicit routing to direct energy to each of the impacters. This property of the selective resonance would be particularly useful in the situation where a number of linear micro vibromotors are implemented in a two-dimensional array in order to position multiple micro components simultaneously. By designing the forward and backward impacters to have

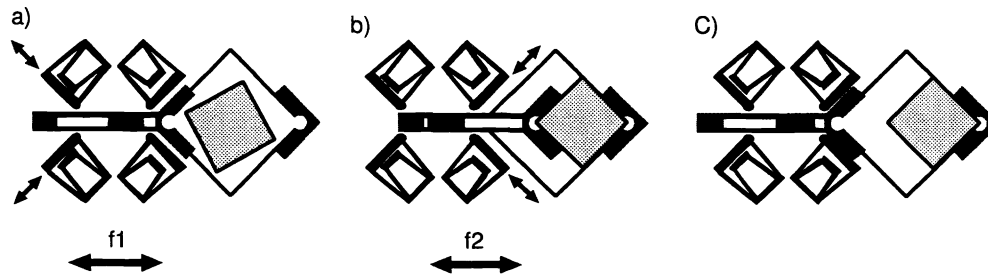


Figure 4. Three-step operation of the externally-resonated linear micro vibromotor. (a) the resonance of forward impacters, (b) the resulting forward sliding motion and the resonance of the backward impacters, (c) the resulting backward sliding motion.

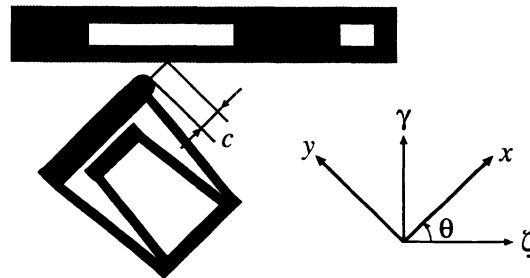


Figure 5. A closed-up view of an impactor mass and the slider side wall.

different resonance frequencies, each linear micro vibromotor in the array can be operated independently by the external piezoelectric vibrations driven by the sum of the signals with appropriate resonance frequencies.³

In Figure 4, note that the direction of the external vibration is *not* parallel to the direction of impacters' oscillation (*i.e.*, the direction of impact). Therefore, it is the component of the external vibration parallel to the direction of impact that causes the resonance in the micro impacters. Another component of external vibration causes the impacters to deform perpendicular to the direction of impact, which is undesirable for efficient operation of the linear micro vibromotor. The micro cantilever impacters, therefore, should have high stiffness in the direction perpendicular to the direction of impact, while keeping the relatively low stiffness in the direction of impact. To achieve this goal, the double-V beam suspension design⁴ is employed in the micro cantilever impacters, which realizes higher transversal stiffness than the conventional folded parallel beam design without affecting the lateral stiffness.⁴

3.2. Modeling

Equations of motions of a lumped parameter model of the impactor-slider system illustrated in Figure 3 is derived in order to obtain an optimal design which maximizes translation speed of the linear slider at desired external input frequencies. Figure 5 shows the closed-up view of an impactor mass and the slider side wall, where (x, y) denote the coordinate system for the impactor position, and (ζ, γ) denote the coordinate system for the slider position. The x - y axes are rotated from ζ - γ axes by the impact angle θ . The following assumptions are made in derivation of the lumped parameter model:

- The impacters and the slider do not move in the direction perpendicular to the substrate.
- The impacters are completely rigid in y direction.
- The slider is completely rigid, and there is no clearance in γ direction between the flange and the slider.

- There is no friction between the substrate and the impacter mass.
- An impact between the impacter mass and the slider side wall occurs instantaneously.
- Impacts by the two impacters in a pair occur simultaneously.

Given these assumptions, an impacter can be modeled as a simple mass-spring-damper system with an external force input $f_{ext}(t)$:

$$m\ddot{x} + b\dot{x} + kx = f_{ext}(t) \quad (1)$$

where m , b , and k are the mass, viscous damping coefficient, and spring constant of a impacter, respectively. Assuming Couette air flow between the substrate and the impacter mass, and small lateral displacement of the folded beams, these parameters are expressed as^{14,4}:

$$m = \rho At + 2 * \rho h w l \quad (2)$$

$$b = \mu \frac{A}{d} \quad (3)$$

$$k = Eh \left(\frac{w}{l}\right)^3 \cos \phi \left(1 + \frac{\cos \phi}{2}\right) \quad (4)$$

where ρ is the mass density of the impacter material (polysilicon); A and t are the planer area (including the area of the joining member of two folded beams) and thickness of the impacter mass, respectively; h , w , and l are the height, width, and total length of the two segments of a V-beam, respectively; μ is the viscosity of the air; d is the vertical gap between the substrate and the impacter mass; E is Young's modulus of the beam material (polysilicon); and ϕ is the half of the angle between the two segments of a V-beam. Assuming the substrate is shaken with the external vibration $\zeta = Z_0 \cos(\omega t)$ in ζ direction, the inertial force $f_{ext}(t)$ exerted to a impacter is:

$$f_{ext}(t) = m\omega^2 Z_0 \cos \theta \cos(\omega t) \quad (5)$$

Similarly, the equation of motion of the linear slider is given as:

$$M\ddot{\zeta} = F(t) \quad (6)$$

where M is the mass of the slider and F is a net force exerted to the slider:

$$F(t) = \begin{cases} 0 & \text{if } \dot{\zeta} = 0 \text{ and } |-B\dot{\zeta} + F_{ext}(t)| < F_s \\ -B\dot{\zeta} + F_{ext}(t) - F_d(\dot{\zeta}/|\dot{\zeta}|) & \text{otherwise} \end{cases} \quad (7)$$

where B is the viscous damping coefficient of the slider; $F_{ext}(t) = M\omega^2 Z_0 \cos(\omega t)$ is the inertial force exerted to the slider; F_s and F_d are static and dynamic frictional forces, respectively. The parameters M and B are given similarly to Equations 2 and 3.

An oblique impact of the impacter tips to the slider side wall is modeled as an impact with restitution in γ direction, and an impact with instantaneous momentum transfer in ζ direction.² Let c be the distance between the impacter tip and the slider side wall measured in x direction as shown in Figure 5. If $x < c$, there is no impact. At $x = c$, the impacter tip contacts the slider sidewall. In in γ direction, the following boundary condition models the energy dissipation of the impacter at an impact:

$$v^+ \sin \theta = -e v^- \sin \theta \quad (8)$$

where v^- and v^+ are impacter velocities in x direction right before and right after the impact, and e is the coefficient of restitution. In ζ direction, linear momentum is transferred from the impacters to the slider. Considering there are two impacters to drive the slider:

$$2mv^+ \cos \theta + MV^+ = 2mv^- \cos \theta + MV^- \quad (9)$$

where V^- and V^+ are slider velocities in x direction right before and right after the impact. Rearranging Equations 8 and 9 gives the boundary condition to model the energy transfer to the slider at an impact:

$$V^+ = V^- + 2\frac{m}{M}(1 + e)v^- \cos \theta \quad (10)$$

Table 1. The physical constant values used in the simulation

Parameter	Value [unit]	Note
ρ	2.33 [g/cm ³]	LPCVD polysilicon ¹⁴
μ	1.79×10^{-5} [Pa · s]	air at 20 C ^o
E	169 [GPa]	Polysilicon ¹⁵
F_s	20 [μ N]	between LPCVD polysilicon layers ¹
F_d	5 [μ N]	between LPCVD polysilicon layers ¹
e	0.5	between LPCVD polysilicon side walls ²

The equations of motion defined as Equations 1 through 10 are numerically integrated with the forth-order Runge Kutta method to predict and optimize a design of the externally-resonated linear micro vibromotor. The values of the ϕ and θ used in the numerical simulation are 15° and 45°, respectively. The values of d , h , and t are constrained by the MUMPs process provided by MCNC used for device fabrication discussed in Section 4. They are set to be 0.75 μ m, 2.0 μ m, and 3.5 μ m, respectively. The physical constant values used in the simulation are shown in Table 1. The values of F_s and F_d account for not only the friction between the substrate and the slider but also the slop between the slider and its guide, and are estimated based on¹ since the slider size and its fabrication process are virtually identical. In order to facilitate fair comparison of device performances with different input frequencies, the power input from the external vibration is kept constant. Since the power input from the external vibration is proportional to $Z_0^2 \cdot \omega^3$, this quantity is kept at a constant value of 50 m²/s³[†].

Figure 6 shows results of numerical integration of the above equations of motion 1 through 10 in the time period from $t_0 = 0.0$ [msec] to $t_f = 3.0$ [msec] with two external input frequencies: (a) $\nu = \omega/2\pi = 5.2$ [kHz] and (b) $\nu = \omega/2\pi = 6.2$ [kHz]. For each input frequency, the top figure shows the time plot of the slider position, and the bottom figure shows the time plot of the impacter position. The parameter values common to both figures are $A = 1.5 \times 10^4$ [μ m²], $w = 4.0$ [μ m], $l = 600$ [μ m], $c = 3.0$ [μ m], and the slider area is 8.0×10^4 [μ m]. These values give the impacter natural frequency $\nu_n = \omega_n/2\pi = 5.2$ [kHz], where $\omega_n = \sqrt{k/m}$. The initial condition $(x(t_0), \dot{x}(t_0))$ is (0.0, 0.0) in both cases. Note that the slider moves approximately *three times* faster when driven with 6.2 kHz (Figure 6 (b)) than when driven with 5.2 kHz, a natural frequency of the impacter (Figure 6 (a)). This increase in the system resonance frequency is due to the nonlinear “hardening spring” behavior observed in many dynamic systems involving impacts^{16–19} often approximated by a damped Duffing oscillator²⁰:

$$\ddot{x} + 2\alpha\dot{x} + \beta x + \epsilon x^3 = f(t) \quad (11)$$

where $\alpha, \beta, \epsilon > 0$ are constants and $f(t)$ is a periodic function of time t .

As other nonlinear oscillatory systems, the Duffing-like nonlinear systems exhibit instabilities where a small perturbation of the initial condition $(x(t_0), \dot{x}(t_0))$ completely changes the frequency response of the system.^{16–19} Such instabilities can occur in the impacter-slider system as defined in Equations 1 through 10, since it is likely that the initial position of the impacter mass varies at every operation of the device due to the sticking between the impacter mass and the substrate, and between the impacter tips and the slider side wall. Figure 7 shows the frequency responses of the impacter-slider system with the same parameter as in Figure 6 with the initial impacter positions $x(t_0) = 0.0, 1.0, 2.0, 3.0$ [μ m]. The system frequency response in this case is the average slider speed during the given time period. Based on the observation that the change in the slider position at an impact is a monotonously increasing function of the linear momentum of the impacters right before the impact, the system response is defined as follows:

$$r(\mathbf{x}_0, \mathbf{p}, \nu) = \frac{\sum_{k=2}^n v^-(t_k)}{t_f - t_0} \quad (12)$$

where $\mathbf{x}_0 = (x(t_0), v(t_0))$ is the initial condition, \mathbf{p} is a vector of the system parameters, ν is the input frequency, n is the number of impacts occurred during the time period from t_0 to t_f , and t_k , $k = 2, 3, \dots, n$ is the time when

[†]For instance, this value gives the external vibration amplitude $Z_0 = 1.27 \mu$ m at the frequency $\nu = \omega/2\pi = 5.0$ kHz, which is reasonable for actuation with a piezoelectric stack vibrator.

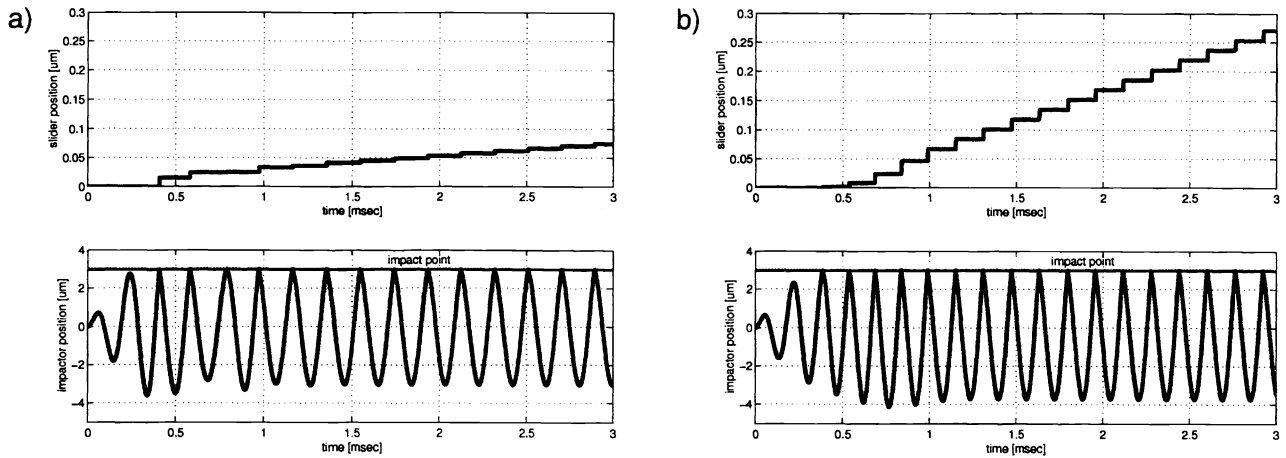


Figure 6. The simulated vibromotor performances. (a) $\nu = \omega/2\pi = 5.2$ [kHz]; and (b) $\nu = \omega/2\pi = 6.2$ [kHz]. The top figure shows the time plot of the slider position, and the bottom figure shows the time plot of the impacter position.

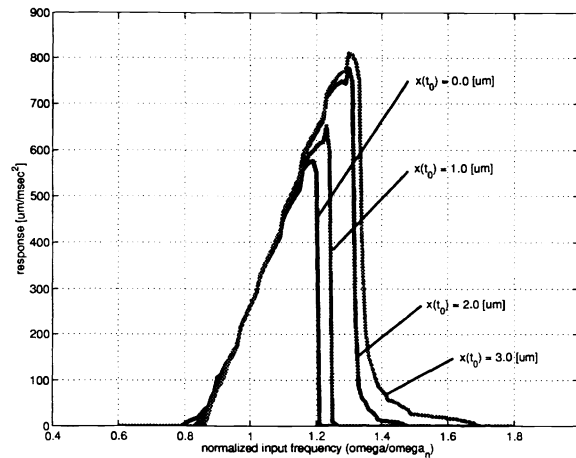


Figure 7. The frequency responses of the impacter-slider system for the initial impacter positions $x(t_0) = 0.0, 1.0, 2.0, 3.0$ [μm].

the second impact, the third impact, *etc.* occurred. Note that $v^-(t_1)$ is *not* included in the above sum to avoid accounting for the first impact due to the initial impacter position. As shown in Figure 7, the input frequencies at which the sudden transitions in the system response occur (bifurcation points²⁰) varies for different initial impacter positions.

Although the above dynamic model shares some similarities to the one presented in *et. al.*¹ there are two essential differences to be noted. First, the model in¹ was solved by piercing together the independently-solved analytical solutions for impact and non-impact cases, whereas the above solution is obtained through numerical integration of the system model. In¹ piercing together two analytical solutions was feasible since the impacter neutral position could be adjusted with the DC bias to the comb actuators such that the impact to the slider side wall occurs *just* at the free oscillation amplitude of the impacters, minimizing the nonlinear effects due to the

impact. On the other hand, the system model needs to be numerically solved in the above since our interest is the full dynamic behavior of the system in “early” impact cases, where the impacts occur far before the impacters reach their free oscillation amplitudes. In such cases, piercing together two analytical solutions cannot predict the dynamic behavior of the system, most notably the nonlinear effects illustrated in Figure 7. Second, in,¹ the slider side wall was modeled as a very stiff spring and a damper, whereas in the above it is modeled as a rigid wall with restitution. Modeling the side wall as a stiff spring and a damper provides a straightforward analytical solution during impact,^{16,17,1} although numerical integration of such a model requires *very* small time step during impact, resulting in increased computational time. On the other hand, the restitution model, employed in numerous work on impact dynamics modeling (*e.g.*,^{18,19,2}) requires much less computational time for numerical integration due to the assumption of the instantaneous impact. The simple restitution model is employed in the above since in our work numerically solving the system model is essential, and also the numerical simulation is repeatedly used during design optimization discusses in the next section.

3.3. Design optimization

The system frequency response as defined in Equation 12 provides an objective function for an optimal vibromotor design that maximizes translation speed of the linear slider at a desired external input frequency. For reliable operation of the device, the design should be optimized for maximum slider speed in the presence of small perturbation of the initial conditions. The instability of the system response illustrated in Figure 7 requires the optimization to maximize the system response at the worst case scenario, *i.e.*, to maximize the minimum response among possible perturbation of the initial condition. In addition, the forward impacters should not respond to the input frequency for the backward impacters, and *vice versa*. These considerations suggest the following max-min formulation of an optimal design problem of the forward impacters:

$$\max_{\mathbf{p}} \min_{\mathbf{x}_0} r(\mathbf{x}_0, \mathbf{p}, \nu_f) \quad (13)$$

$$\text{s.t.} \quad \max_{\mathbf{x}_0} r(\mathbf{x}_0, \mathbf{p}, \nu_b) = 0 \quad (14)$$

$$\mathbf{x}_0 \in D \quad (15)$$

$$\mathbf{p} \in P \quad (16)$$

where r is the system frequency response as defined in Equation 12, and ν_f and ν_b are the input frequencies for the forward and backward impacters, respectively. Equation 14 constraints that a feasible design should not respond to the backward input frequency ν_b regardless of the initial condition \mathbf{x}_0 . Switching ν_f in Equation 13 and ν_b in Equation 14 gives a formulation for the backward impacters.

Note that the evaluation of $r(\mathbf{x}_0, \mathbf{p}, \nu)$ requires *only* the impacter dynamics as defined in Equations 1, 4, 5, and 8. The design parameters \mathbf{p} , therefore, only consists of the ones for the impacters: the planer area A of the impacter mass; the width w and the total length l of the two segments of a V-beam; and the distance c between the impacter tip and the slider side wall measured in x direction. The lower bounds of these parameters are given by the impacter geometry illustrated in Figure 5 and the minimum feature length $2.0 \mu m$, as specified by the MUMPS process. Since these parameters are not upper bounded, the set P is defined as follows:

$$P = \{(A, w, l, c) \mid 20.0 \leq A < \infty, 2.0 \leq w < \infty, 8.0 \leq l < \infty, 2.0 \leq c < \infty\} \quad (17)$$

It is assumed that the perturbation in the initial condition is only in the initial impacter position due to the sticking between the impacter mass and the substrate and between the impacter mass and the slider side wall, and is bounded by $-c$ and c . In other words,

$$D = \{(x(t_0), v(t_0)) \mid -c \leq x(t_0) \leq c, v(t_0) = 0\} \quad (18)$$

Using $r(\mathbf{x}_0, \mathbf{p}, \nu)$ as an objective function rather than more direct measures of the slider speed, *e.g.*, $\zeta(t_f)$, has two practical advantages for design optimization. First, the evaluation of r is far less computationally expensive than the evaluation of the quantities involving the slider dynamics such as $\zeta(t_f)$. Second, the prediction of the device performance based on r is not necessarily less accurate than the prediction based on the slider dynamics, since it does not involve phenomenological constants such as F_d and F_s , whose accurate estimates are extremely difficult to obtain.

Table 2. Result from an optimization for $\nu_f = 6.0$ [kHz] and $\nu_b = 3.0$ [kHz].

Parameter [unit]	Forward impacter	Backward impacter
A [μm]	13544	45446
w [μm]	5.6774	4.0354
l [μm]	795.74	795.27
c [μm]	5.2046	2.6676
ν_n [kHz]	5.8199	2.0385
$x(t_0)$ [μm]	-2.6000	-2.6676

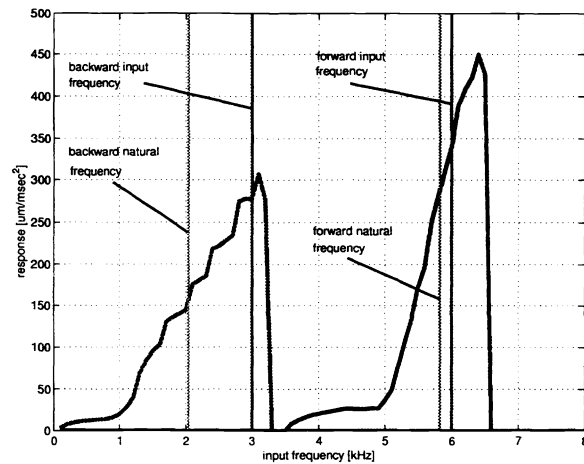


Figure 8. Frequency responses of the forward (right) and backward (left) impacters optimized for $\nu_f = 6.0$ [kHz] and $\nu_b = 3.0$ [kHz].

Since the gradient-based nonlinear programming algorithms²¹ fail due to the discontinuous change in the system response illustrated in Figure 7, the above optimization problem is solved using the Simulated Annealing algorithm.²² Table 2 shows the result from an optimization of the forward and backward impacters for the forward input frequency $\nu_f = 6.0$ [kHz] and the backward input frequency $\nu_b = 3.0$ [kHz]. Note that the initial impacter position $x(t_0)$ of the forward impacter that gives minimum response is approximately $-0.5c$, not the minimum possible value $-c$ as for the backward impacter. This contradicts the trend illustrated in Figure 7, where the system response becomes smaller as $x(t_0)$ decreases. Further analyses reveal that for $-c \leq x(t_0) < -0.5c$, the first impact due to the large initial deflection triggers bifurcation in the response which results in the response larger than for $x(t_0) = -0.5c$.

Figure 8 shows the frequency responses of the forward (right) and backward (left) impacters in Table 2. Also plotted on the figure are the forward and backward input frequencies, and the natural frequencies of the optimal impacters. It can be easily seen from the figure that the shapes and the relative location of the two response curves are optimized such that the forward impacter has a maximum response at the forward input frequency while achieving zero response at the backward input frequency, and *vice versa*.

4. FABRICATION AND TESTING

Prototypes of externally-resonated linear micro vibromotors are fabricated using the three-layer polysilicon surface micro machining process provided by the MCNC MUMPS service, where the bottom polysilicon layer serves as a ground plane, and the middle and the top polysilicon layers are used for micro mechanical structures. Figure 9

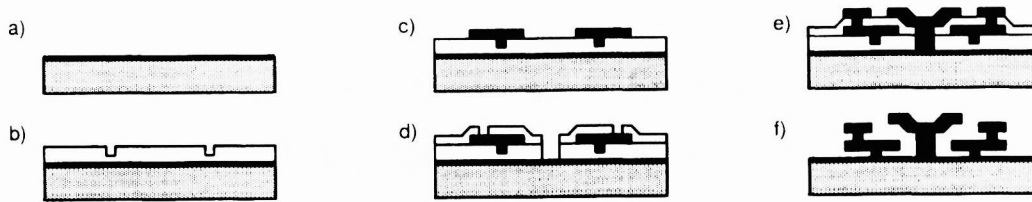


Figure 9. A basic flow of the MUMPS process. (a) Deposit and pattern the bottom polysilicon layer; (b) Deposit and pattern the first PSG sacrificial layer; (c) Deposit and pattern the middle polysilicon layer; (d) Deposit and pattern the second PSG sacrificial layer; (e) deposit and pattern the top polysilicon layer; (f) Dissolve the sacrificial layers in HF solution.

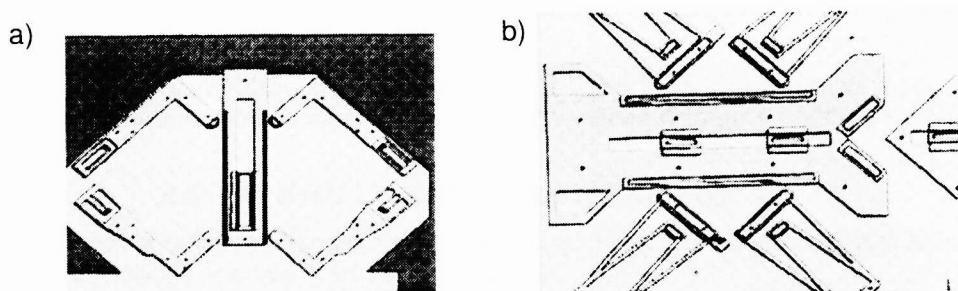


Figure 10. Fabricated prototypes of the externally-resonated to linear micro vibromotor with approximately $600\ \mu\text{m}$ in the slider length. Preliminary testing suggested the several modifications to produce the design configuration shown in Figures 3.

illustrates a basic flow of the MUMPS process[†]. A series of figures shows transversal cross sections of the micro linear slider being fabricated. First, the bottom polysilicon layer (referred to as Poly0) is deposited and patterned on a silicon substrate using low pressure chemical vapor deposition (LPCVD), as shown in Figure 9 (a). This is followed by the deposition and patterning of a $0.75\ \mu\text{m}$ thick sacrificial layer of LPCVD phosphosilicate glass (PSG). Dimples are wet etched on this PSG layer to reduce friction between the bottom and middle polysilicon layers at the completion of the fabrication process (Figure 9 (b)). On top of the PSG layer, a $2.0\ \mu\text{m}$ thick LPCVD polysilicon layer (referred to as Poly1) is deposited and patterned. Figure 9 (c) shows the cross sectional pattern of the slider made of Poly1. After the deposition and patterning of another PSG sacrificial layer (shown in Figure 9 (d)), and a $1.5\ \mu\text{m}$ polysilicon layer (referred to as Poly2: shown in Figure 9 (e)), the PSG layers are dissolved in an etching solution (HF), releasing the mechanical structure made of Poly1 and Poly2 (Figure 9 (f)).

Prior to the fabrication of the optimal device designs, two types of prototypes are fabricated for preliminary testing, whose photos are shown in Figure 10. These prototypes are tested for the forward and backward motion via external vibration applied by an piezoelectric stack vibrator glued to the dice with dry epoxy. This preliminary testing suggested the several modifications to produce the design configuration shown in Figure 3. Figure 11 show a mask layout of an array of these devices, each optimized for a different input frequency, with “dummy” micro components. The size of the dummy square components is $500\ \mu\text{m} \times 500\ \mu\text{m}$, made with Poly1 layer in the MUMPS process. These dummy micro components are anchored to the substrate with a very thin polysilicon structure which can be easily broken with a probe tip at the testing. The fabrication of these devices are currently in progress. Upon the completion of fabrication, testing is to be done on the positioning and release of the dummy micro components against the anchored fixture elements, as well as on the cross talk among the impacters of different vibromotors on a substrate.

[†]See <http://mems.mcnc.org/mumps.html> for details.

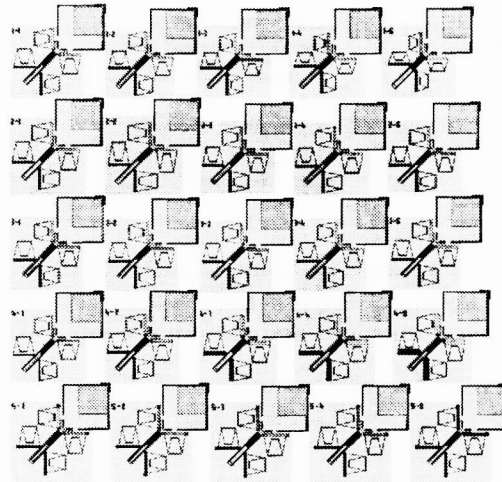


Figure 11. An array of the externally-resonated micro vibromotors with “dummy” micro components, each of which is optimized for a different input frequency. The size of the square micro components is $500\ \mu\text{m} \times 500\ \mu\text{m}$.

5. DISCUSSION AND FUTURE WORK

This work presented design, analysis, and optimization of a linear micro vibromotor for on-substrate fine positioning of micro-scale components, where a micro linear slider is actuated by vibratory impacts exerted by micro cantilever impacters. These micro cantilever impacters are *selectively* resonated by shaking the entire substrate with a piezoelectric vibrator, requiring no need for built-in driving mechanisms such as electrostatic comb actuators as reported previously.^{1,2} This selective resonance of the micro cantilever impacters via an external vibration energy field³ provides with a very simple means of controlling forward and backward motion of the micro linear slider, facilitating *assembly and disassembly* of a micro component on a substrate. An analytical model of the device is derived in order to obtain, through the Simulated Annealing algorithm, an optimal design which maximizes translation speed of the linear slider at desired external input frequencies. Prototypes of the externally-resonated linear micro vibromotor are fabricated using the three-layer polysilicon surface micro machining process provided by the MCNC MUMPS service.

As discussed in Section 1, gross positioning of a micro component needs to be done prior to on-substrate fine positioning using an externally-resonated linear micro vibromotor. Although the gross positioning could be done sequentially in pick-and-place fashion, vibratory palletization,²³ a part orienting method common to centimeter-scale mechanical parts, could provide *very* efficient means of parallel gross positioning of micro components. During the palletization, surface adhesion forces can be virtually eliminated by applying vertical vibration in ultrasonic range as recently reported in.¹⁰ Such vertical vibration can also facilitate the operation of the linear micro vibromotor by reducing the friction between a micro component and the substrate.

The current fine positioning scheme, however, lacks a positive fastening means to secure the attachment of the component to the substrate. Therefore, the design modification of the linear slider, the etched cavity, and/or anchored fixture should be investigated in order to achieve selective fastening and release of a component. For this, the application of removable micro mechanical latching fasteners, or micro “mouse traps,”²⁴ will be considered as a possible fastening means.

One of the most promising applications of the micro assembly/disassembly as described in this paper is bare-chip interconnection in multi-chip module (MCM), which requires a precision assembly/disassembly of meso-scale components with high density electrical interconnection. Although the chips currently used in MCMs are typically in 5–10 mm scale, the advent of the assembly/disassembly method by using the externally-resonated linear micro vibromotor presented in this paper would stimulate further *disintegration* of subsystem components to improve the overall system modularity, which in turn would reduce the sizes of the components to be assembled.

ACKNOWLEDGMENTS

This work was carried out using facilities at the Computational Design Laboratory and MEMS Laboratory in the Department of Mechanical Engineering and Applied Mechanics, the University of Michigan. These sources of support are gratefully acknowledged.

REFERENCES

1. M. Daneman, N. Tien, O. Solgaard, A. Pisano, K. Lau, and R. Muller, "Linear microvibromotor for positioning optical components," *Journal of Microelectromechanical Systems* **5**, pp. 159–165, September 1996.
2. A. Lee and A. Pisano, "Polysilicon angular microvibromotors," *Journal of Microelectromechanical Systems* **1**, pp. 70–76, June 1992.
3. T. Yasuda, I. Shimoyama, and H. Miura, "Microrobot actuated by a vibration energy field," *Sensors and Actuators A* **43**, pp. 366–370, 1994.
4. L. Saggere, S. Kota, and S. Crary, "A new design for suspension systems of linear microactuators," in *Proceedings of the 1994 ASME International Mechanical Engineering Congress and Exposition*, vol. DSC 55-2, pp. 671–675, 1994.
5. C. Keller and R. Howe, "Hexsil tweezers for teleoperated microassembly," in *Microelectromechanical Systems*, pp. 72–77, IEEE, 1997.
6. R. Fearing, "Survey of sticking effects for micro parts handling," in *Microelectromechanical Systems*, pp. 212–217, IEEE, 1995.
7. H. Yeh and J. Smith, "Fluidic self-assembly of GaAs microstructures on Si substrates," *Sensors and Materials* **6**(6), pp. 319–332, 1994.
8. M. Cohn, C.-J. Kim, and A. Pisano, "Self-assembling electrical networks: an application of micromachining technology," in *Transducers '91: 1991 IEEE International Conference on Solid-State Sensors and Actuators*, pp. 490–493, 1991.
9. K. Hosokawa, I. Shimoyama, and H. Miura, "Two-dimensional micro-self-assembly using the surface tension of water," in *IEEE Microelectromechanical Systems*, 1996.
10. K. Böhringer, K. Goldberg, M. Cohn, R. Howe, and A. Pisano, "Parallel microassembly with electrostatic force fields," in *Proceeding of the 1997 IEEE International Conference on Robotics and Automation*, IEEE, 1997.
11. M. Judy, Y.-H. Cho, R. Howe, and A. Pisano, "Self-adjusting microstructures (SAMS)," in *IEEE Micro Electro Mechanical Systems*, pp. 51–56, 1991.
12. S. Burgett, K. Pister, and R. Fearing, "Three dimensional structures made with microfabricated hinges," in *ASME International Mechanical Engineering Congress and Exposition*, pp. 1–11, 1992.
13. R. Prasad, K.-F. Böhringer, and N. MacDonald, "Design, fabrication, and characterization of single crystal silicon latching snap fasteners for micro assembly," in *Proceedings of the ASME International Mechanical Engineering Congress and Exposition*, 1995.
14. Y.-H. Cho, A. Pisano, and R. Howe, "Viscous damping model for laterally oscillating microstructures," *Journal of Microelectromechanical Systems* **3**, pp. 81–87, June 1994.
15. J. Sharpe, B. Yuan, and R. Vaidyanathan, "Measurements of Young's modulus, Poisson's ratio, and tensile strength of polysilicon," in *Proceedings of the IEEE Microelectromechanical Systems*, pp. 424–429, 1996.
16. S. Shaw and P. Holmes, "A periodically forced piecewise linear oscillator," *Journal of Sound and Vibration* **90**(1), pp. 129–155, 1983.
17. S. Shaw, "Forced vibrations of a beam with one-sided amplitude constraint: theory and experiment," *Journal of Sound and Vibration*, pp. 199–211, 1985.
18. M. Heiman, P. Sherman, and A. Bajaj, "On the dynamics and stability of an inclined impact pair," *Journal of Sound and Vibration* **114**(3), pp. 535–547, 1987.
19. T. Dalrymple, "Numerical solutions to vibroimpact via an initial value problem formulation," *Journal of Sound and Vibration* **132**(1), pp. 19–32, 1989.
20. S. Strogatz, *Nonlinear Dynamics and Chaos: with Applications to Physics, Biology, Chemistry, and Engineering*, Addison Wesley, Reading, Massachusetts, 1994.
21. P. Papalambros and D. Wilde, *Principles of Design Optimization*, Cambridge University Press, 1985.
22. S. Kirkpatrick, C. Gellat, and M. Vecchi, "Optimization by simulated annealing," *Science* **220**, pp. 671–680, 1983.
23. P. Moncevicz, M. Jakiela, and K. Ulrich, "Orientation and insertion of randomly presented parts using vibratory agitation," in *Proceedings of the ASME 3rd Conference on Flexible Assembly Systems*, DE-Vol. 33, pp. 41–47, 1991.
24. K. Saitou and M. Jakiela, "Design of a self-closing compliant "mouse trap" for micro assembly," in *Proceedings of the 1996 ASME International Mechanical Engineering Congress and Exposition*, DSC-Vol. 59, pp. 421–426, 1996.